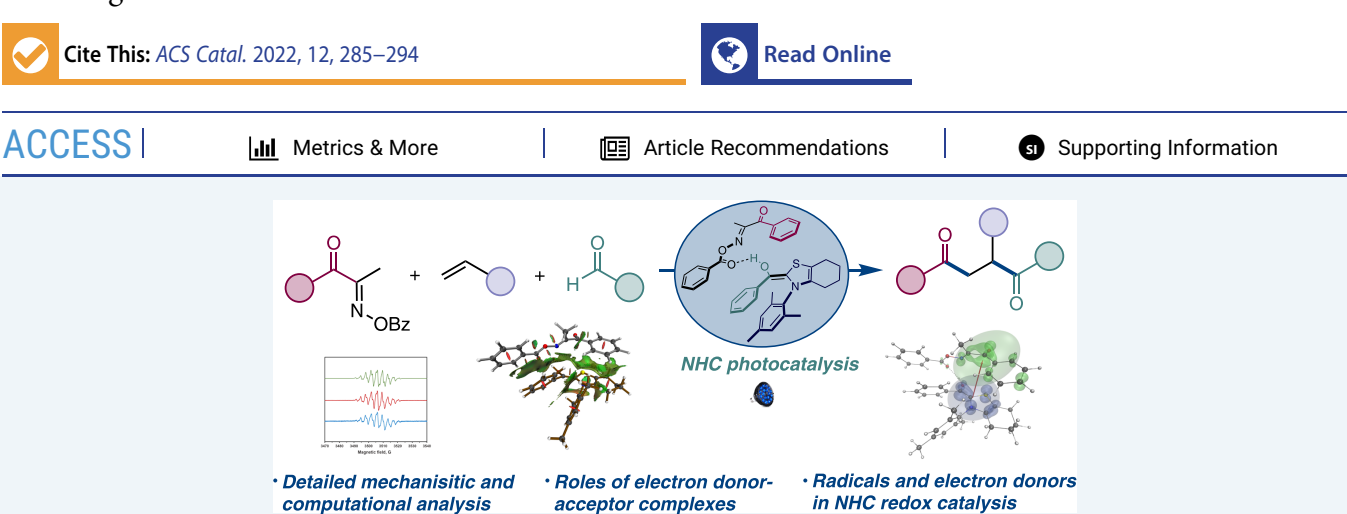


Research Article pubsiacs.org/acscatalysis

N-Heterocyclic Carbene-Photocatalyzed Tricomponent Regioselective 1,2-Diacylation of Alkenes Illuminates the Mechanistic Details of the Electron Donor-Acceptor Complex-**Mediated Radical Relay Processes**

Shengfei Jin,[†] Xianwei Sui,[†] Graham C. Haug,[†] Viet D. Nguyen, Hang T. Dang, Hadi D. Arman, and Oleg V. Larionov*



ABSTRACT: Progress in the development of photocatalytic reactions requires a detailed understanding of the mechanisms underpinning the observed reactivity, yet mechanistic details of many photocatalytic systems, especially those that involve electron donor-acceptor complexes, have remained elusive. We report herein the development and a combined mechanistic and computational study of photocatalytic alkene 1,2-diacylation that enables a regioselective installation of two different acyl groups, establishing direct, tricomponent access to 1,4-diketones, key intermediates in heterocyclic and medicinal chemistry. The studies revealed the central role of the electron donor-acceptor complex formed from an N-heterocyclic carbene (NHC) catalyst-derived intermediate and an acyl transfer reagent, providing a detailed description of the structural and electronic factors determining the characteristics of the photoinduced charge-transfer process that mediates photocatalytic transformation. The in-depth investigation also illuminated the roles of other radical intermediates and electron donors relevant to the catalytic activities of N-heterocyclic carbenes in radical reactions

acceptor complexes

KEYWORDS: charge transfer, 1,2-diacylation, N-heterocyclic carbenes, photocatalysis, radical addition

INTRODUCTION

Photocatalysis has recently emerged as one of the most enabling methodological advances in organic synthesis, streamlining the introduction of diverse functional groups into unactivated substrates and increasing the efficiency of functional group interconversions.² Despite the rapid progress in the development of new photocatalytic reactions, their mechanistic understanding has been lagging because of the complexity of catalytic processes.

computational analysis

Recent studies showed that a number of novel synthetic transformations can be enabled by photochemically or thermally induced electron donor-acceptor (EDA or charge transfer) complexes,^{3,4} adding to the trove of knowledge on the importance of EDA complexes in organic and organometallic reactions.⁵ The formation of a charge-transfer encounter complex is typically manifested by the appearance of charge-

transfer bands in the near-ultraviolet (UV), visible, or nearinfrared (IR) regions of the absorption spectra of solutions of electron donors and acceptors. 5f The charge-transfer encounter complex can undergo an interfragment electron transfer (IFCT) with thermal activation if the electron transfer takes place over an accessible electron-transfer barrier. Alternatively, photoexcitation can be used to overcome an inefficient thermal ET process to access the electron-transfer state that, upon thermal

Received: October 6, 2021 Revised: December 2, 2021 Published: December 15, 2021





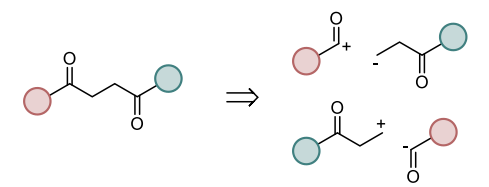
relaxation, can dissociate into separated ion radicals or undergo subsequent transformations (Figure 1).

Electron Donor-Acceptor (EDA) complex-mediated reactivity

$$\begin{array}{c} \begin{array}{c} \begin{array}{c} \begin{array}{c} \\ \end{array} \\ \end{array} \end{array} \begin{array}{c} \begin{array}{c} \\ \end{array} \\ \end{array} \begin{array}{c} \\ \end{array} \end{array} \begin{array}{c} \\ \end{array} \end{array} \begin{array}{c} \\ \end{array} \end{array} \begin{array}{c} \\ \end{array} \end{array} \begin{array}{c} \\ \end{array} \end{array} \begin{array}{c} \\ \end{array} \begin{array}{c} \\ \end{array} \begin{array}{c} \\ \end{array} \begin{array}{c} \\ \end{array} \end{array} \begin{array}{c} \\ \end{array} \begin{array}{c} \\ \end{array} \begin{array}{c} \\ \end{array} \end{array} \begin{array}{c} \\ \end{array} \end{array} \begin{array}{c} \\ \end{array} \end{array} \begin{array}{c} \\ \end{array} \end{array} \begin{array}{c} \\ \end{array} \begin{array}{c} \\ \end{array} \begin{array}{c} \\ \end{array} \end{array} \begin{array}{c} \\ \end{array} \begin{array}{c} \\ \end{array} \\ \end{array} \begin{array}{c} \\ \end{array} \begin{array}{c} \\ \end{array} \begin{array}{c} \\ \end{array} \begin{array}{c} \\ \end{array} \\ \end{array} \begin{array}{c} \\ \end{array} \begin{array}{c} \\ \end{array} \\ \end{array} \begin{array}{c} \\ \end{array} \begin{array}{c} \\ \end{array}$$

N-Heterocyclic carbene redox catalysis

Challenge: efficient regioselective construction of 1,4-dicarbonyls



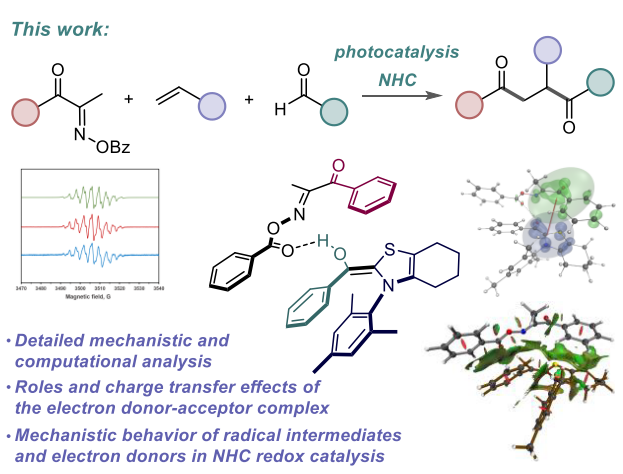


Figure 1. N-Heterocyclic carbene-photocatalyzed regioselective alkene 1,2-diacylation.

N-heterocyclic carbenes (NHC) have recently emerged as versatile catalysts for a variety of photocatalytic transformations. In particular, reactions that involve Breslow intermediates I as electron donors have enabled new radical functionalizations (Figure 1).^{6,7} The reactions are thought to proceed via a thermal or photoinduced electron transfer from Breslow intermediates I or their deprotonated forms, and the involvement of EDA complexes was inferred based on the changes in the absorption spectra for some of the reactions. However, mechanistic details of the reactions and the roles of various electron donors and radical intermediates remain poorly understood.

1,4-Dicarbonyl compounds are centrally important synthetic intermediates that provide access to a variety of nitrogen, oxygen, and sulfur heterocycles, as well as other diverse products with applications in medicinal chemistry and materials science.8 However, the synthesis of 1,4-dicarbonyls remains challenging because of the mismatch in the polarity-driven reactivities of the carbonyl precursors (Figure 1).

Tricomponent regioselective 1,2-diacylation of alkenes, wherein two different acyl groups are appended to an alkene in a regioselective manner, can provide a new approach to 1,4dicarbonyl compounds. However, 1,2-diacylation of alkenes remains underdeveloped, 10 and a general method that enables a regioselective installation of two different acyl groups by 1,2diacylation has been elusive.

We report herein the development of a tricomponent, photocatalytic, regioselective alkene 1,2-diacylation that proceeds via a photoinduced proton-coupled electron transfer in an EDA complex formed from an acyl transfer reactant and a Breslow intermediate. We provide a detailed mechanistic and computational analysis of the key roles played by the EDA complex and other intermediates that may guide the development of other photoinduced and thermal NHC catalytic reactions driven by a single electron transfer from Breslow intermediates.

RESULTS AND DISCUSSION

Optimization studies with oxime 1a, styrene 2a, and aldehyde 3a revealed that tricomponent coupling is readily enabled in the presence of precatalyst C1 under blue light-emitting diode (LED) ($\lambda = 450 \text{ nm}$) and at 65 °C (Table 1, entry 1). The

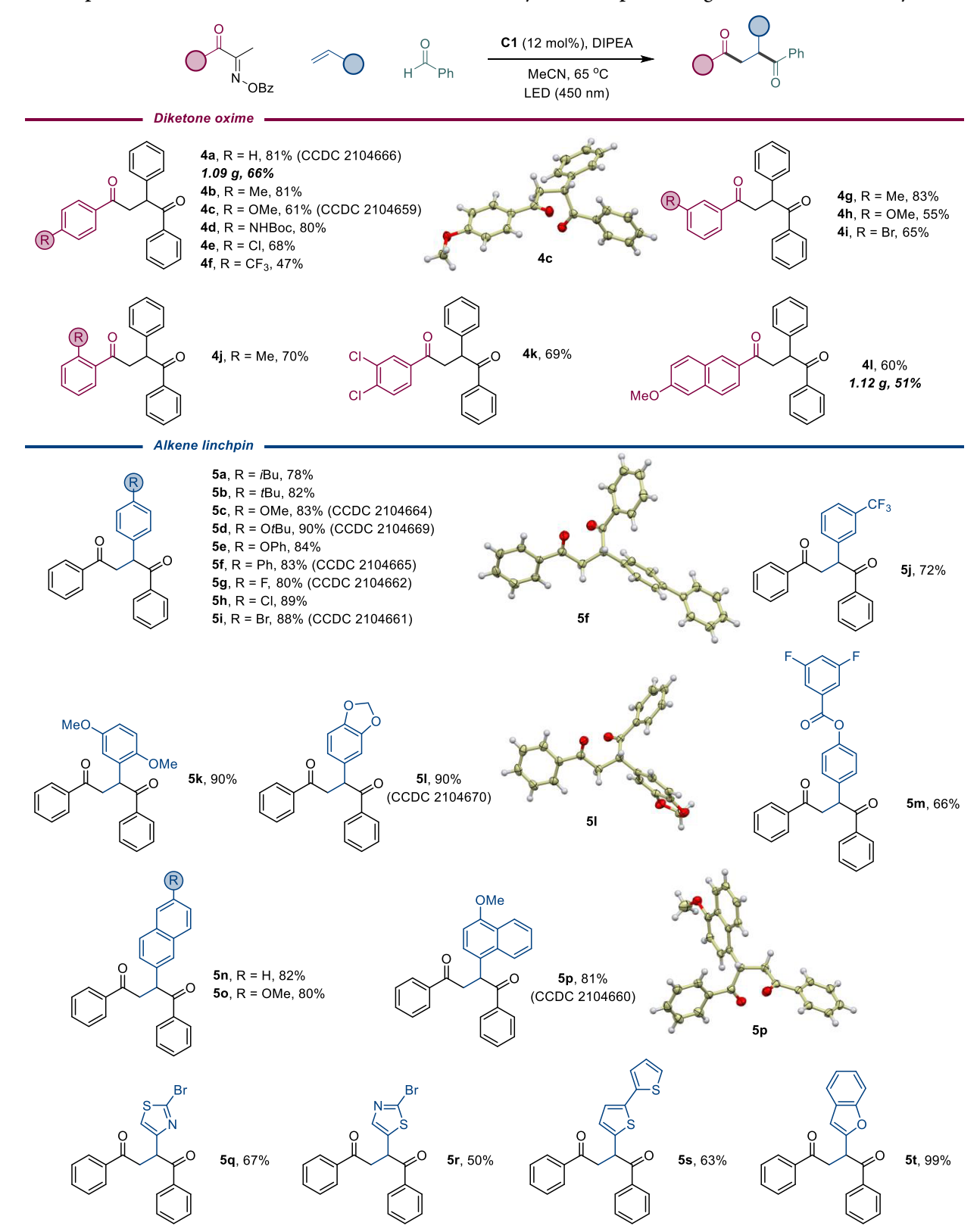
Table 1. Reaction Conditions for the Visible Light-Induced Dual Catalytic Alkenylation

entry	change from optimal conditions	yield, % ^b
1	no change	83 (81°)
2	no light	7
3	400 nm instead of 450 nm LED	53
4	ambient temperature	9
5	no C1	0
6	C2 instead of C1	0
7	C3 instead of C1	55
8	C4 instead of C1	53
9	PhCH ₃ instead of MeCN	53
10	DMF instead of MeCN	64
11	under air	39

^aReaction conditions: oxime 1a (0.2 mmol), styrene (2a) (0.4 mmol), benzaldehyde (3a) (0.4 mmol), C1 (12 mol %), DIPEA (0.4 mmol), MeCN (2.6 mL), LED (450 nm), 65 °C, and 16 h. ^bDetermined by ¹H NMR with 1,3,5-trimethoxybenzene as an internal standard. ^cIsolated yield.

reaction did not proceed without light and was less efficient at shorter wavelengths (entries 2, 3). An elevated temperature was also required to effect the conversion to ketone 4a (entry 4). No conversion was observed without the catalyst (entry 5), while the size of the carbocyclic moiety in the carbene catalyst had a significant effect on the catalytic performance, with the fivemembered ring derivative C2 being completely devoid of the catalytic activity and a reduced performance for the seven- and

Table 2. Scope of Oxime Precursors and Alkenes in the Photocatalytic Tricomponent Regioselective Alkene Diacylation^a



^aSee Table 1 for reaction conditions.

eight-membered congeners C3 and C4 (entries 6-8). Furthermore, both less polar and more polar solvents were detrimental to the reaction performance (entries 9 and 10). Finally, a diminished yield was observed, when the reaction was

carried out under air, pointing to the detrimental effects of oxygen as an oxidant.

The scope of the reaction was examined next with a range of oxime precursors and (hetero)aromatic alkenes (Table 2).

Table 3. Scope of Aldehydes in the Photocatalytic Tricomponent Regioselective Alkene Diacylation^a

^aSee Table 1 for reaction conditions.

A variety of products were produced in good yields from diverse oxime precursors (4a-4l). Both electron-donating and electron-withdrawing substituents were tolerated, including alkyl (4b, 4g, and 4j), methoxy (4c and 4h), amide (4d), chloro, and bromo (4e, 4i, and 4k) groups without any detrimental dehalogenation, as well as the naphthalene core (4l) and the medically important trifluoromethyl group (4f). Similarly, an array of diversely substituted styrenes was readily converted to the corresponding 1,4-diketone products (5a-5t). The reaction performed well with electron-rich (5a-5f and 5k-5m) and electron-deficient (5g-5j) arylalkenes, including naphthalene derivatives (5n-5p). Notably, nitrogen-, oxygen-, and sulfur-containing heterocyclic groups were introduced into the 1,4-diketone framework (5q-5t).

The scope of aldehydes was investigated next (Table 3). A diverse range of products was accessed, revealing good functional group tolerance, for example, with respect to alkyl, alkoxy, amide, and halogen groups (6a-6l). Other aromatic and heteroaromatic aldehydes, including naphthalene (6m and 6n), pyridine (60-6q), indole (6r and 6s), benzofuran (6t), and thiophene (6u) were equally suitable, also highlighting the stability of the reaction bromoarene functionality to dehalogenation induced by single electron transfer (SET). Several products were accessed in gram quantities (4a, 4l, and 6o), underscoring the synthetic utility of the method. Importantly, the acceptor-derived acyl group was added to the less-substituted position in the alkene, while the aldehyde-derived

acyl group was appended to the more-substituted terminus in all of the products, as revealed by the X-ray crystallographic analysis of products 4a, 4c, 5c, 5d, 5f, 5g, 5i, 5l, 5p, 6l, and 6n. We proceeded further with the investigation of the reaction mechanism.

A radical trapping experiment with (2,2,6,6-tetramethylpiperidin-1-yl)oxidanyl (TEMPO) showed that the production of diketone 7 is completely suppressed in the presence of TEMPO (Scheme 1). The formation of the acyl radical trapping products 8 and 9 in nearly equal amounts supports the intermediacy of species capable of transferring an acyl radical (e.g., *m*-methoxybenzoyl radical from the oxime precursor and an

Scheme 1. TEMPO Radical Trapping Experiment

oxidized Breslow intermediate derived from benzaldehyde, vide infra).

UV/visible (vis) spectroscopic studies indicated that none of the reactants (1a-3a, C1, N, N-diisopropylethylamine, DIPEA) or reagents absorb in the visible range.

(Figures 2 and S1). Similarly, no appreciable increase in absorption was observed for combinations of oxime 1a, alkene

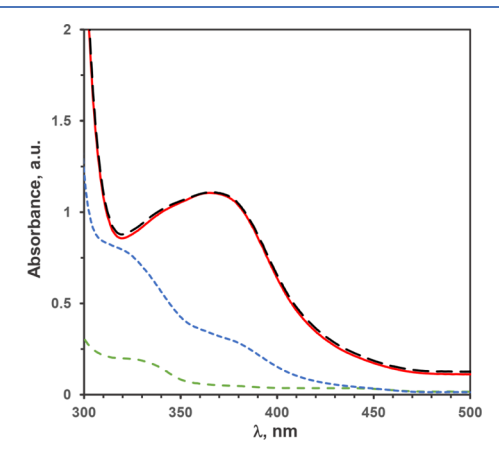


Figure 2. Absorption spectra of the acetonitrile solutions of the reaction mixture at the concentrations specified below (black lines); oxime 1a, aldehyde 3a, C1, and DIPEA (red lines); C1, DIPEA, and aldehyde 3a (blue lines); C1 and DIPEA (green lines). Concentrations: oxime 1a (1.2 mM), aldehyde 3a (3.6 mM), alkene 2a (3.6 mM), C1 (1.2 mM), and DIPEA (12 mM).

2a, and aldehyde 3a, or C1 and DIPEA. Interestingly, new absorption bands were observed for a solution of aldehyde 3a,

C1, and DIPEA, suggesting the formation of Breslow intermediate 10.¹¹ Furthermore, spectroscopic studies revealed a substantially stronger absorption in the near-UV and visible range for a solution of oxime 1a, aldehyde 3a, C1, and DIPEA.

The strong absorption was also observed in the reaction mixture. Taken together, these results indicate that the reaction proceeds via the formation of an EDA complex between the Breslow intermediate and electron acceptor 1a that subsequently undergoes fragmentation, producing the prerequisite acyl radical intermediate. This conclusion was further supported by mass spectrometric studies that revealed the presence of species with the molecular masses corresponding to intermediate $10 \ (364.1730, [M+H^+])$ and the complex of $10 \ \text{with}$ oxime $1a \ (653.2458 \ [M+Na^+])$.

Density functional theory (DFT) and time-dependent-DFT (TD-DFT) studies were carried out next to clarify the mechanism of the EDA complex-mediated 1,2-diacylation process (Figure 3). The addition of carbene 11 to aldehyde 3a can produce E- and Z-isomers of the Breslow intermediate. Z-isomer 10 is more stable by ~2.6 kcal/mol, indicating that it is the major component in the equilibrium. Both catalyst 11 and intermediate 10 are relatively weak reductants ($E_{\rm red}(11^{+}/11) = 1.65$ V and $E_{\rm red}(10^{+}/10) = -0.37$ V vs SCE in MeCN) that cannot mediate a thermodynamically favorable reduction of oxime 1a ($E_{\rm red}(1a^{+}/1a) = -1.29$ V), in agreement with earlier studies, pointing to insufficient reducing power of Breslow intermediates in the context of redox-mediated NHC-catalyzed processes. ¹²

Complexation of intermediate 10 with oxime 1a by hydrogen bonding proceeds nearly isergonically ($\Delta G = 0.32 \text{ kcal/mol}$), supporting the facile formation of complex 12 in the reaction

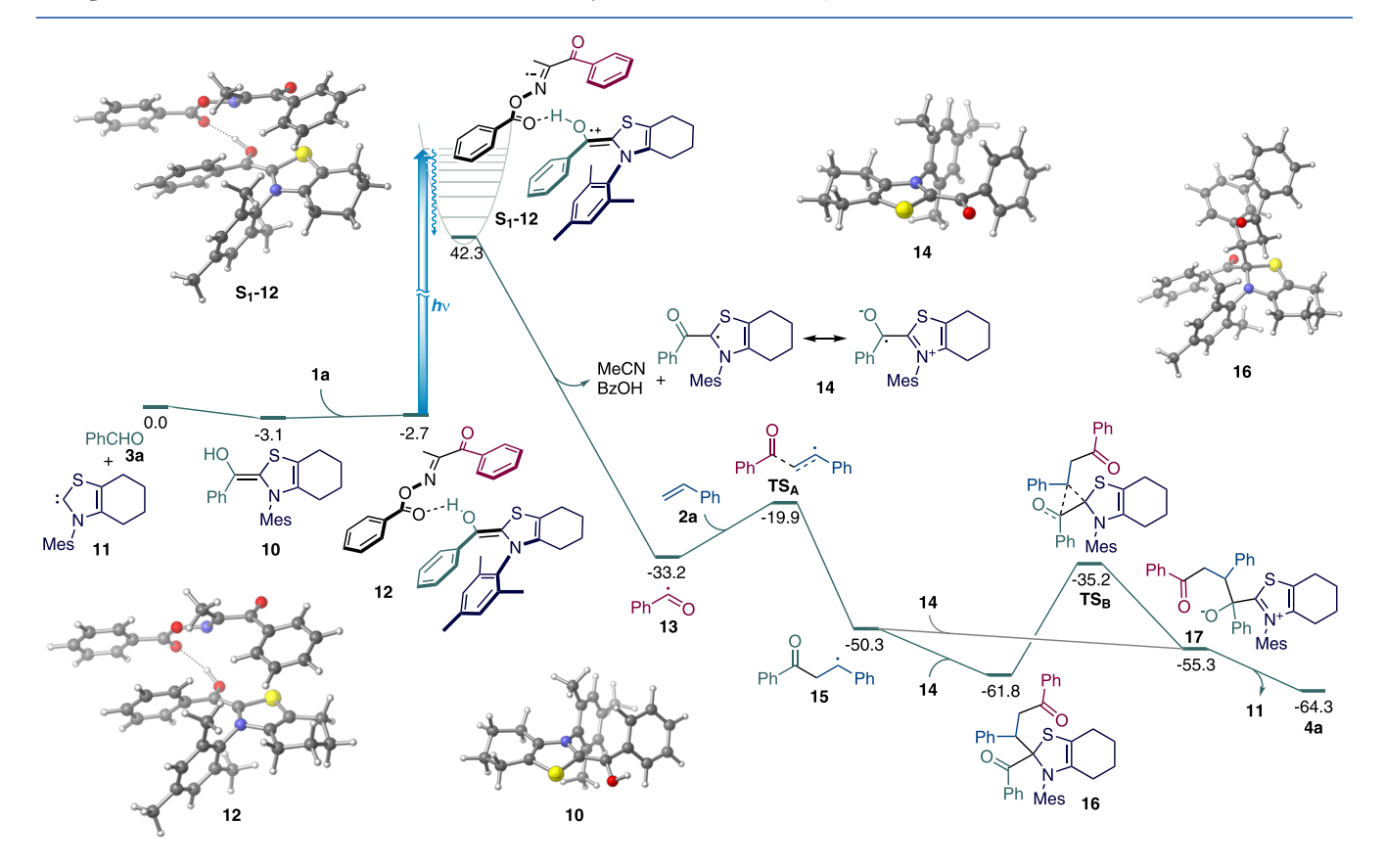


Figure 3. Computed Gibbs free energy profile for the regional formula 1,2-diacylation of alkenes (ΔG , kcal/mol). Mes = mesityl.

system. Furthermore, the noncovalent interaction (NCI) plot ¹³ points to the extensive noncovalent interactions between the phenyl ring of the acyl fragment in acceptor **1a** and the bicyclic system of intermediate **10** on one terminus, as well as the *N*-benzoyloxy moiety of acceptor **1a** and the phenyl ring of the enol moiety in intermediate **10** on the other terminus, in addition to the hydrogen bond, as key stabilizing interactions between the two components of complex **12** (Figure 4A). The stabilizing

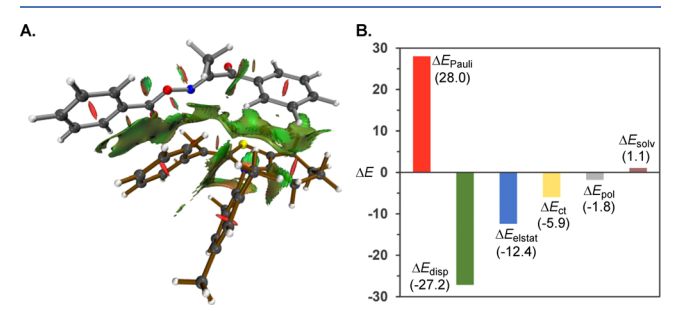


Figure 4. (A) NCI plot of complex 12 formed from Breslow intermediate 10 (brown) and acceptor 1a (gray). (B) Energy decomposition analysis (ALMO-EDA) of complex 12.

noncovalent interactions of the acyl fragment with the aliphatic ring of the NHC fragment are particularly noteworthy, given the significant difference in the catalytic performance of NHC catalysts with varied aliphatic ring sizes (cf. entries 1, 6–8, Table 1). The importance of the noncovalent interactions for the stabilization of complex 12 is further evident from the energy decomposition analysis based on absolutely localized molecular orbitals (ALMO-EDA, Figure 4B) that points to a large contribution of the stabilizing dispersion energy ($\Delta E_{\rm disp}$) to the interaction energy ($\Delta E_{\rm int}$) that alone nearly compensates for the Pauli (steric) repulsion ($\Delta E_{\rm Pauli}$). Notably, TD-DFT calculations of the absorption spectra of catalyst 11, intermediate 10, and complex 12 show substantial differences (Figure 5). While

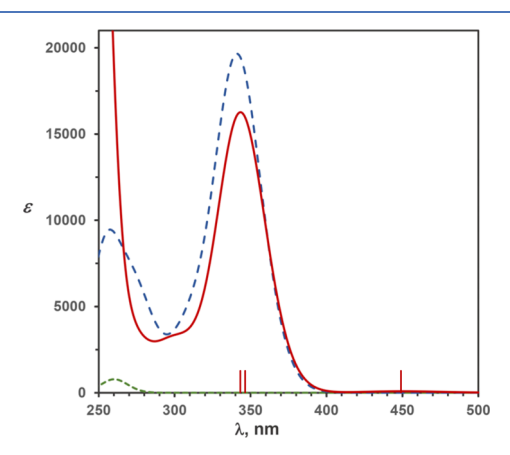


Figure 5. Calculated absorption spectra of catalyst **11** (--, green), intermediate **10** (--, blue), and complex **12** (---, red). Vertical lines indicate λ_{max} for the absorptions in the UV-A/vis range for complex **12**.

no absorption bands were observed in the near-UV and visible range for catalyst 11, strong absorption appeared in the spectrum of intermediate 10, consistent with the experimentally observed spectral data for model Breslow intermediate systems. 11

For intermediate 10, the peak with $\lambda_{max} = 343$ nm corresponded to the electron transitions from the highest

occupied molecular orbital (HOMO) that is located on the enol moiety to the lowest unoccupied molecular orbital (LUMO) located on the phenyl ring (Figure 6A). By contrast, for complex

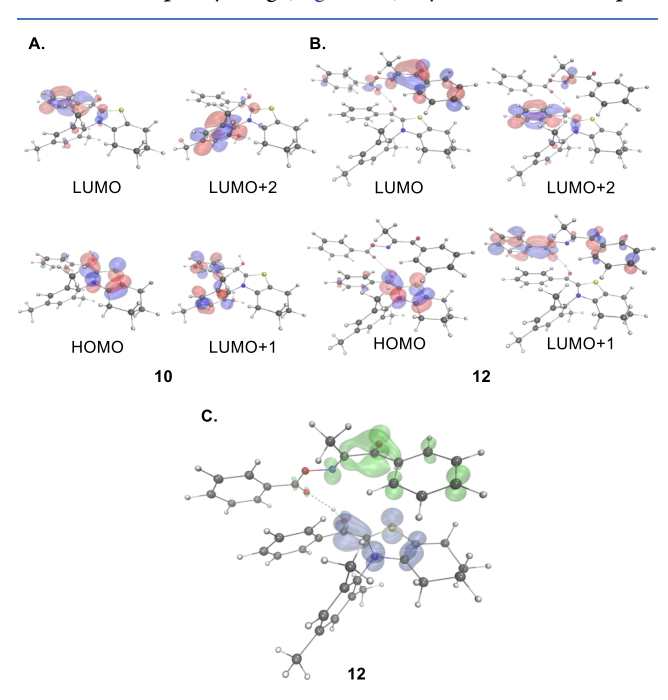


Figure 6. HOMOs and the three LUMOs of intermediate **10** (A) and complex **12** (B) with an isovalue of 0.05 a.u.; the electron—hole analysis of complex **12**, isovalue 0.005 a.u. (C).

12, the lowest energy band with λ_{max} = 449 nm corresponded to the interfragment $\pi \to \pi^*$ charge-transfer electron transitions from the HOMO located on the enol moiety of the Breslow intermediate to the LUMO and LUMO+1 located on the oxime acceptor (Figure 6B). Significantly, the transition to the LUMO that is located on the oxime-acyl fragment exhibits the largest contribution (96%). The IFCT analysis 15 indicates that the excitation results in a nearly complete (98%) charge transfer from the Breslow intermediate fragment to the acceptor 1a fragment. The excitation was further examined by an electron hole analysis, 15,16 revealing the significantly separated hole (corresponding to the HOMO) and the electron (corresponding to the LUMO) with the substantial distance between the centroids of the hole and the electron (D = 3.89 Å) and H = 2.64Å, reflecting the broad distribution of the hole and electron (Figure 6C). Furthermore, the relatively large t index (2.33 Å) points to a notable hole/electron separation with a small overlap $(S_r = 0.12 \text{ a.u.})$. In addition, two higher-intensity absorptions contribute to the band in the near-UV region with λ_{max} = 347 nm and 342 nm. The band with $\lambda_{\rm max}$ = 347 nm corresponds to the π $\rightarrow \pi^*$ electron transitions from the HOMO to LUMO+1 and LUMO+2 localized on the acceptor 1a fragment (both the benzoate and the acyl moieties) for LUMO+1, and mostly the phenyl group in the carbene fragment (with a smaller contribution of the oxime moiety in 1a) for LUMO+2. The IFCT transition provided a smaller but still the most significant contribution (76%). The shorter-wavelength excitation (λ_{max} = 343 nm) had significant contributions from $\pi \to \pi^*$ transitions from the HOMO to higher energy unoccupied orbitals with a much smaller contribution (22%) of the IFCT. The TD-DFT calculations are consistent with the experimental data and observations and provide important insights into the involvement of EDA complex 12 in the reaction. The experimental spectra of the mixtures of acceptor 1a, C1, DIPEA, and aldehyde 3a exhibit bands in the near-UV region that are consistent with calculations. Furthermore, the position of the charge-transfer band with $\lambda_{\rm max}=449$ nm in the visible spectrum is congruent with the experimentally determined optimal irradiation wavelength ($\lambda_{\rm max}=450$ nm). In addition, the significant contribution of the oxime moiety to the LUMO of complex 12 and the nearly complete electron transfer to the LUMO may facilitate the elimination of the benzoate and fragmentation

of acceptor 1a. The relatively low calculated absorptivity (ε = 86 M⁻¹·cm⁻¹) for the charge-transfer band suggests that it likely overlaps with the substantially stronger near-UV-centered absorption tailing into the visible region that can also mediate the reaction pathway because of the high contribution of the IFCT (vide supra). The differences in the relative intensities of the calculated and experimental absorption bands for intermediate 10 and complex 12 can be due to the underestimation of the oscillator strengths of the charge-transfer excitations for 12 compared to the local excitations for 10, as well as the presence of the vibronic structure in the experimental spectra. 17 Importantly, TD-DFT calculations further indicate that the HOMO \rightarrow LUMO singlet excited state S_1-12 lies 45.0 kcal/mol above the ground state, making it thermally inaccessible at the reaction conditions and indicating that photoactivation is required to mediate charge transfer, in line with experimental observations. Subsequent proton shift from the OH group of the Breslow intermediate fragment to the carbonyl oxygen of the benzoate moiety in the acceptor 1a can facilitate the elimination of the benzoate and fragmentation of acceptor 1a.

Subsequent fragmentation of singlet excited state S₁-12 proceeds highly exergonically, affording acyl radical 13, as well as acetonitrile, benzoic acid, and acyl-NHC radical 14 (Figure 3). The natural bond orbital (NBO) analysis ¹⁸ of radical **14** points to the relatively low spin density on the carbonyl carbon atom (0.1398) with significant delocalization of the residual spin density over the carbonyl oxygen (0.2446), as well as the NHC core (S1: 0.1618, C2: 0.1971, N3: 0.1938, C5: 0.1017, Figure 7A), as previously observed for other radicals of this type. 12a Experimentally, the intermediacy of radical 14 was confirmed by electron paramagnetic resonance (EPR) studies of the reaction mixture (Figure 7B). The radical was also independently generated via the acylthiazolium intermediate obtained in a reaction of carbene 11 with benzoyl chloride and subsequent reduction with zinc. The addition of acyl radical 13 to alkene 2a proceeds exergonically over a small barrier (13.3 kcal/mol), producing radical 15 (Figure 3). Given the significant delocalization of the spin density in NHC radical 14, the cross-termination of radicals 14 and 15 can take place at the carbon atom in the S-C-N moiety of the NHC fragment in 14, producing NHC adduct 16, or directly at the carbonyl C atom, leading to carbonyl adduct 17, with estimates of the transitionstate energies pointing to the addition at the S-C-N moiety in 14 as being more kinetically favorable (See the Supporting Information). As was also observed for a similar system by Scheidt and Cheong, 61 NHC adduct 16 can undergo a rearrangement to carbonyl adduct 17. The availability of the $16 \rightarrow 17$ isomerization pathway for NHC catalyst 11 suggests that this mechanism can also play significant roles in other NHC-catalyzed radical reactions.

NHC redox-catalyzed reactions have been reported to proceed under thermal and photochemical conditions, and, in

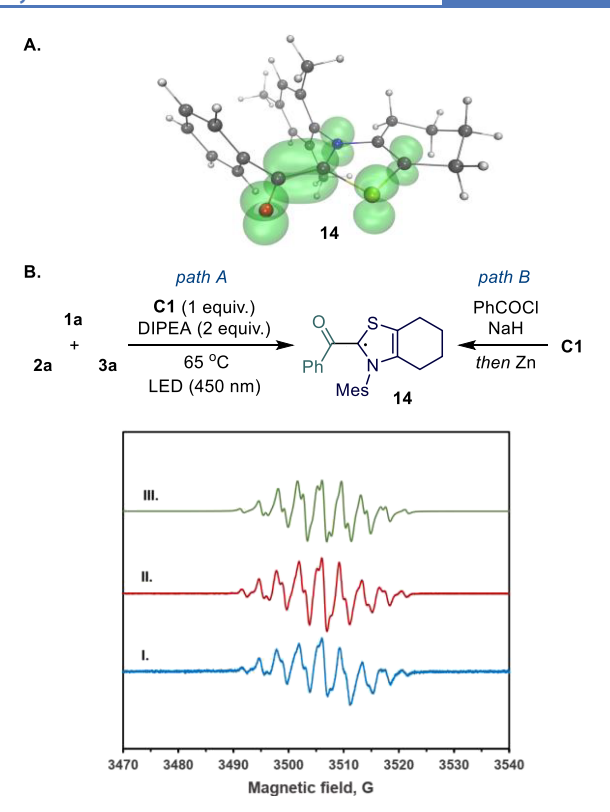


Figure 7. (A) Computed NBO spin density (isovalue 0.005 a.u.) in radical intermediate **14.** (B) Room temperature X-band EPR spectroscopic study of radical **14** in the 1,2-diacylation reaction. **I.** Reaction mixture of the 1,2-diacylation reaction (path A). **II.** Generation of radical **14** via the acylthiazolium intermediate reduction (path B). **III.** Simulated EPR spectrum. g = 2.0052; $a_{\rm N} = 3.45$ G, $a_{\rm H} = 3.30$ (2 H), 3.70 (2 H), 4.50 G (2 H).

some cases, with the involvement of EDA complexes, suggesting that a range of inner and outer-sphere electron-transfer processes may be operative, depending on the reaction conditions and the nature of electron acceptors. 6b-o Given the importance of the donor-acceptor interactions for the feasibility of the thermal and photoinduced electron transfer from Breslow intermediates, for example, as observed in 1,2diacylation and the previously described systems, 7b-e the potential involvement of other Breslow intermediate-derived species as outer-sphere electron donors in the NHC redoxcatalyzed reactions that are typically performed in the presence of relatively weak bases (e.g., amines) was also examined. Although anion 18 was found to be a sufficiently strong reductant (E(14/18) = -1.73 V) to mediate an outer-sphere electron transfer to the typical organic electron acceptors used in the NHC-catalyzed radical processes (e.g., N-hydroxyphthalimide esters and easily reducible haloarenes), the low acidity of intermediate 10 (p K_a = 36.1 in MeCN) suggests that the formation of anion 18 (Figure 8) is significantly disfavored with the typical bases used for the reactions (e.g., $pK_{BH}^{+} = 24.3$ for DBU and 18.8 for triethylamine in MeCN¹⁹), if other more thermodynamically accessible electron donors are formed under the reaction conditions. Indeed, a hydrogen bond complex 19 is readily accessible by an exergonic reaction of intermediate 10 and DBU ($\Delta G = -1.7 \text{ kcal/mol}$) and is also a sufficiently strong reductant $(E_{red}(14 + DBU-H^+/19) = -1.23 \text{ V})$ that can mediate single electron transfer to the acceptor substrates by multisite proton-coupled electron transfer (PCET) (Figure 8A). In the case of the 1,2-diacylation reaction, however, the

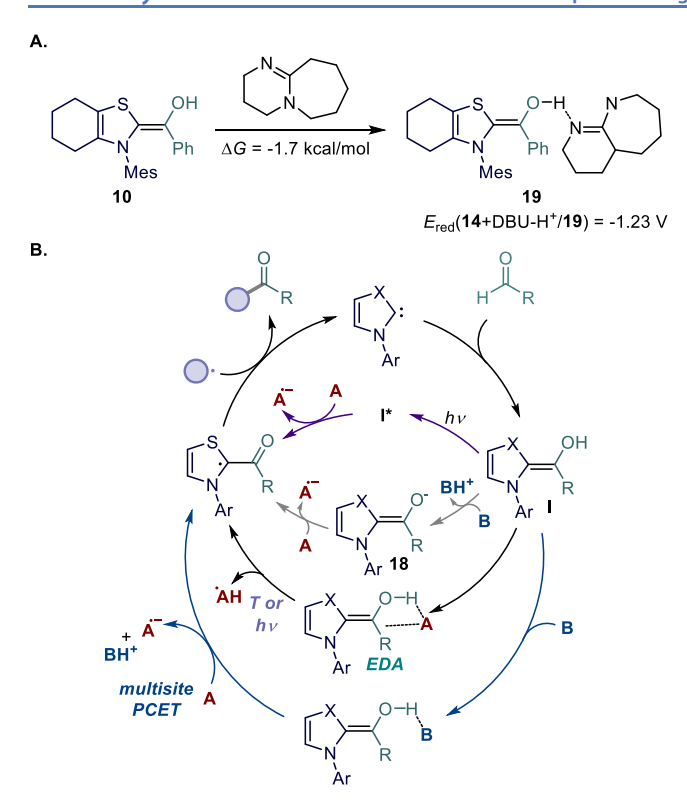


Figure 8. (A) Formation of acid—base complex **19.** (B) Mechanistic manifold for the NHC redox catalysis.

formation of the corresponding complex of intermediate 10 with DIPEA $(E_{red}(14 + DIPEA-H^+/10-DIPEA) = -1.30 \text{ V})$ is substantially disfavored ($\Delta G = 5.2 \text{ kcal/mol}$) so that this reduction pathway does not participate in 1,2-diacylation. In addition, photoexcited Breslow intermediate I* may also mediate electron transfer.²⁰ Our studies show that single electron transfer from the triplet excited state of intermediate **10** is exergonic $(E_{red}(10^{+}./T_1-10) = -1.92 \text{ V})$. However, the calculated molar absorptivity of intermediate 10 at 450 nm is substantially lower than that for complex 12 $(\log(\varepsilon_{12}/\varepsilon_{10}) =$ 4.3), indicating that the pathway may not be providing a significant contribution to 1,2-diacylation. These results indicate that a range of Breslow intermediate-derived species can participate in the NHC-catalyzed radical processes, including EDA complexes (e.g., 12), as well as hydrogen bond complexes (e.g., 19), and the type of the electron-transfer process and the activation mode (thermal or photochemical, outer or inner sphere) are determined by the structural and redox properties of the acceptor substrates and catalysts (Figure 8B).

CONCLUSIONS

In summary, we have developed a visible light-induced, *N*-heterocyclic carbene-catalyzed regioselective 1,2-diacylation of alkenes that affords direct access to 1,4-diketones via a tricomponent C—C bond-forming radical coupling. Mechanistic and computational studies provided a detailed description of the EDA complex between the Breslow intermediate and the oxime acceptor that is central to the observed reactivity and the stabilizing interactions, notably dispersion, within the complex. The studies have revealed the key role of the interfragment charge transfer in enabling the otherwise thermally inaccessible process. Our mechanistic investigation also clarified the roles of the radical acyl transfer species and various single electron

donors in NHC redox catalysis, highlighting the roles of the EDA and PCET channels in facilitating key redox processes.

ASSOCIATED CONTENT

Supporting Information

The Supporting Information is available free of charge at https://pubs.acs.org/doi/10.1021/acscatal.1c04594.

Experimental and spectral details for all new compounds and all reactions reported, and details of computational studies (PDF)

X-ray crystallographic data (ZIP)

AUTHOR INFORMATION

Corresponding Author

Oleg V. Larionov — Department of Chemistry, The University of Texas at San Antonio, San Antonio, Texas 78249, United States; orcid.org/0000-0002-3026-1135; Email: oleg.larionov@utsa.edu

Authors

Shengfei Jin — Department of Chemistry, The University of Texas at San Antonio, San Antonio, Texas 78249, United States; Present Address: Wuya College of Innovation, Shenyang Pharmaceutical University, Shenyang, Liaoning 110,016, P. R. China (S.J.)

Xianwei Sui — Department of Chemistry, The University of Texas at San Antonio, San Antonio, Texas 78249, United States

Graham C. Haug – Department of Chemistry, The University of Texas at San Antonio, San Antonio, Texas 78249, United States

Viet D. Nguyen – Department of Chemistry, The University of Texas at San Antonio, San Antonio, Texas 78249, United States

Hang T. Dang — Department of Chemistry, The University of Texas at San Antonio, San Antonio, Texas 78249, United States

Hadi D. Arman – Department of Chemistry, The University of Texas at San Antonio, San Antonio, Texas 78249, United States

Complete contact information is available at: https://pubs.acs.org/10.1021/acscatal.1c04594

Author Contributions

[†]S. J., X.S., and G.C.H. contributed equally to this work.

Notes

The authors declare no competing financial interest.

ACKNOWLEDGMENTS

Financial support by the NSF (CHE-1455061) is gratefully acknowledged. The UTSA NMR and X-ray crystallography facilities were supported by the NSF (CHE-1625963 and CHE-1920057).

REFERENCES

(1) (a) Skubi, K. L.; Blum, T. R.; Yoon, T. P. Dual Catalysis Strategies in Photochemical Synthesis. *Chem. Rev.* **2016**, *116*, 10035–10074. (b) Twilton, J.; Le, C.; Zhang, P.; Shaw, M. H.; Evans, R. W.; Macmillan, D. W. C. The Merger of Transition Metal and Photocatalysis. *Nat. Rev. Chem.* **2017**, *1*, No. 0052. (c) Chuentragool, P.; Kurandina, D.; Gevorgyan, V. Catalysis with Palladium Complexes

Photoexcited by Visible Light. Angew. Chem., Int. Ed. 2019, 58, 11586–11598.

- (2) (a) Corey, E. J.; Cheng, X. M., The Logic of Chemical Synthesis; Wiley: 1989; (b) Crossley, S. W. M.; Shenvi, R. A. A Longitudinal Study of Alkaloid Synthesis Reveals Functional Group Interconversions as Bad Actors. Chem. Rev. 2015, 115, 9465–9531.
- (3) (a) Arceo, E.; Jurberg, I. D.; Álvarez-Fernández, A.; Melchiorre, P. Photochemical Activity of a Key Donor-Acceptor Complex Can Drive Stereoselective Catalytic α -Alkylation of Aldehydes. *Nat. Chem.* **2013**, 5, 750-756. (b) Kandukuri, S. R.; Bahamonde, A.; Chatterjee, I.; Jurberg, I. D.; Escudero-Adán, E. C.; Melchiorre, P. X-Ray Characterization of an Electron Donor-Acceptor Complex that Drives the Photochemical Alkylation of Indoles. Angew. Chem., Int. Ed. 2015, 54, 1485-1489. (c) Zhang, J.; Li, Y.; Xu, R.; Chen, Y. Donor-Acceptor Complex Enables Alkoxyl Radical Generation for Metal-Free C(sp³)-C(sp³) Cleavage and Allylation/Alkenylation. Angew. Chem., Int. Ed. 2017, 56, 12619-12623. (d) Morack, T.; Mück-Lichtenfeld, C.; Gilmour, R. Bioinspired Radical Stetter Reaction: Radical Umpolung Enabled by Ion-Pair Photocatalysis. Angew. Chem., Int. Ed. 2019, 58, 1208-1212. (e) Cong, F.; Lv, X.-Y.; Day, C. S.; Martin, R. Dual Catalytic Strategy for Forging sp²-sp³ and sp³-sp³ Architectures via β -Scission of Aliphatic Alcohol Derivatives. J. Am. Chem. Soc. 2020, 142, 20594-20599. (f) de Pedro Beato, E.; Spinnato, D.; Zhou, W.; Melchiorre, P. A General Organocatalytic System for Electron Donor-Acceptor Complex Photoactivation and Its Use in Radical Processes. J. Am. Chem. Soc. 2021, 143, 12304-12314. (g) Kammer, L. M.; Badir, S. O.; Hu, R.-M.; Molander, G. A. Photoactive Electron Donor-Acceptor Complex Platform for Ni-Mediated $C(sp^3)-C(sp^2)$ Bond Formation. Chem. Sci. 2021, 12, 5450-5457. (h) Lipp, A.; Badir, S. O.; Dykstra, R.; Gutierrez, O.; Molander, G. A. Catalyst-Free Decarbonylative Trifluoromethylthiolation Enabled by Electron Donor-Acceptor Complex Photoactivation. Adv. Synth. Catal. 2021, 363, 3507-3520. (i) Polites, V. C.; Badir, S. O.; Keess, S.; Jolit, A.; Molander, G. A. Nickel-Catalyzed Decarboxylative Cross-Coupling of Bicyclo [1.1.1]pentyl Radicals Enabled by Electron Donor-Acceptor Complex Photoactivation. Org. Lett. 2021, 23, 4828-4833. (j) Ward, R. M.; Schomaker, J. M. Allene Trifunctionalization via Amidyl Radical Cyclization and TEMPO Trapping. J. Org. Chem. 2021, 86, 8891-8899. (k) Liu, B.; Lim, C.-H.; Miyake, G. M. Light-Driven Intermolecular Charge Transfer Induced Reactivity of Ethynylbenziodoxol(on)e and Phenols. J. Am. Chem. Soc. 2018, 140, 12829-12835.
- (4) (a) Lima, C. G. S.; de M. Lima, T.; Duarte, M.; Jurberg, I. D.; Paixão, M. W. Organic Synthesis Enabled by Light-Irradiation of EDA Complexes: Theoretical Background and Synthetic Applications. ACS Catal. 2016, 6, 1389–1407. (b) Crisenza, G. E. M.; Mazzarella, D.; Melchiorre, P. Synthetic Methods Driven by the Photoactivity of Electron Donor–Acceptor Complexes. J. Am. Chem. Soc. 2020, 142, 5461–5476.
- (5) (a) Bunnett, J. F. Aromatic Substitution by the S_{RN}¹ Mechanism. *Acc. Chem. Res.* 1978, 11, 413–420. (b) Fukuzumi, S.; Mochida, K.; Kochi, J. K. A Unified Mechanism for Thermal and Photochemical Activation of Charge-Transfer Processes with Organometals. Steric Effects in the Insertion of Tetracyanoethylene. *J. Am. Chem. Soc.* 1979, 101, 5961–5972. (c) Fox, M. A.; Younathan, J.; Fryxell, G. E. Photoinitiation of the S_{RN}1 Reaction by Excitation of Charge-Transfer Complexes. *J. Org. Chem.* 1983, 48, 3109–3112. (d) Patz, M.; Fukuzumi, S. Electron Transfer in Organic Reactions. *J. Phys. Org. Chem.* 1997, 10, 129–137. (e) Rathore, R.; Kochi, J. K. Donor/Acceptor Organizations and the Electron-Transfer Paradigm for Organic Reactivity. *Adv. Phys. Org. Chem.* 2000, 35, 193–318. (f) Rosokha, S. V.; Kochi, J. K. Fresh Look at Electron-Transfer Mechanisms via the Donor/Acceptor Bindings in the Critical Encounter Complex. *Acc. Chem. Res.* 2008, 41, 641–653.
- (6) (a) Ishii, T.; Kakeno, Y.; Nagao, K.; Ohmiya, H. N-Heterocyclic Carbene-Catalyzed Decarboxylative Alkylation of Aldehydes. *J. Am. Chem. Soc.* **2019**, *141*, 3854–3858. (b) Dai, L.; Xia, Z.-H.; Gao, Y.-Y.; Gao, Z.-H.; Ye, S. Visible-Light-Driven N-Heterocyclic Carbene Catalyzed γ and ϵ -Alkylation with Alkyl Radicals. *Angew. Chem., Int.*

- Ed. 2019, 58, 18124-18130. (c) Ishii, T.; Ota, K.; Nagao, K.; Ohmiya, H. N-Heterocyclic Carbene-Catalyzed Radical Relay Enabling Vicinal Alkylacylation of Alkenes. J. Am. Chem. Soc. 2019, 141, 14073-14077. (d) Song, R.; Chi, Y. R. N-Heterocyclic Carbene Catalyzed Radical Coupling of Aldehydes with Redox-Active Esters. Angew. Chem., Int. Ed. 2019, 58, 8628-8630. (e) Bayly, A. A.; McDonald, B. R.; Mrksich, M.; Scheidt, K. A. High-Throughput Photocapture Approach for Reaction Discovery. Proc. Natl. Acad. Sci. U S. A. 2020, 117, 13261. (f) Kakeno, Y.; Kusakabe, M.; Nagao, K.; Ohmiya, H. Direct Synthesis of Dialkyl Ketones from Aliphatic Aldehydes through Radical N-Heterocyclic Carbene Catalysis. ACS Catal. 2020, 10, 8524-8529. (g) Li, J.-L.; Liu, Y.-Q.; Zou, W.-L.; Zeng, R.; Zhang, X.; Liu, Y.; Han, B.; He, Y.; Leng, H.-J.; Li, Q.-Z. Radical Acylfluoroalkylation of Olefins through N-Heterocyclic Carbene Organocatalysis. Angew. Chem., Int. Ed. 2020, 59, 1863-1870. (h) Ota, K.; Nagao, K.; Ohmiya, H. N-Heterocyclic Carbene-Catalyzed Radical Relay Enabling Synthesis of δ -Ketocarbonyls. Org. Lett. 2020, 22, 3922-3925. (i) Bay, A. V.; Fitzpatrick, K. P.; González-Montiel, G. A.; Farah, A. O.; Cheong, P. H.-Y.; Scheidt, K. A. Light-Driven Carbene Catalysis for the Synthesis of Aliphatic and α -Amino Ketones. Angew. Chem., Int. Ed. 2021, 60, 17925-17931. (j) Chen, L.; Jin, S.; Gao, J.; Liu, T.; Shao, Y.; Feng, J.; Wang, K.; Lu, T.; Du, D. N-Heterocyclic Carbene/Magnesium Cocatalyzed Radical Relay Assembly of Aliphatic Keto Nitriles. Org. Lett. 2021, 23, 394-399. (k) Gao, Y.; Quan, Y.; Li, Z.; Gao, L.; Zhang, Z.; Zou, X.; Yan, R.; Qu, Y.; Guo, K. Organocatalytic Three-Component 1,2-Cyanoalkylacylation of Alkenes via Radical Relay. Org. Lett. 2021, 23, 183-189. (1) Li, Z.; Huang, M.; Zhang, X.; Chen, J.; Huang, Y. N-Heterocyclic Carbene-Catalyzed Four-Component Reaction: Chemoselective Cradical-Cradical Relay Coupling Involving the Homoenolate Intermediate. ACS Catal. 2021, 11, 10123-10130. (m) Liu, M.-S.; Min, L.; Chen, B.-H.; Shu, W. Dual Catalysis Relay: Coupling of Aldehydes and Alkenes Enabled by Visible-Light and NHC-Catalyzed Cross-Double C-H Functionalizations. ACS Catal. 2021, 11, 9715-9721. (n) Liu, W.; Vianna, A.; Zhang, Z.; Huang, S.; Huang, L.; Melaimi, M.; Bertrand, G.; Yan, X. Mesoionic Carbene-Breslow Intermediates as Super Electron Donors: Application to the Metal-Free Arylacylation of Alkenes. Chem Catal. 2021, 1, 196-206. (o) Matsuki, Y.; Ohnishi, N.; Kakeno, Y.; Takemoto, S.; Ishii, T.; Nagao, K.; Ohmiya, H. Aryl Radical-Mediated N-Heterocyclic Carbene Catalysis. Nat. Commun. 2021, 12, 3848. (p) Sato, Y.; Goto, Y.; Nakamura, K.; Miyamoto, Y.; Sumida, Y.; Ohmiya, H. Light-Driven N-Heterocyclic Carbene Catalysis Using Alkylborates. ACS Catal. 2021, 12886-12892. (q) Kusakabe, M.; Nagao, K.; Ohmiya, H. Radical Relay Trichloromethylacylation of Alkenes through N-Heterocyclic Carbene Catalysis. Org. Lett. 2021, 23, 7242-7247. (r) Zuo, Z.; Daniliuc, C. G.; Studer, A. Cooperative NHC/ Photoredox Catalyzed Ring-Opening of Aryl Cyclopropanes to 1-Aroyloxylated-3-Acylated Alkanes. Angew. Chem., Int. Ed. 2021, 60, 25252.
- (7) (a) Ishii, T.; Nagao, K.; Ohmiya, H. Recent Advances in N-Heterocyclic Carbene-Based Radical Catalysis. Chem. Sci. 2020, 11, 5630-5636. (b) Liu, J.; Xing, X.-N.; Huang, J.-H.; Lu, L.-Q.; Xiao, W.-J. Light opens a new window for *N*-heterocyclic carbene catalysis. *Chem.* Sci. 2020, 11, 10605-10613. (c) Ohmiya, H. N-Heterocyclic Carbene-Based Catalysis Enabling Cross-Coupling Reactions. ACS Catal. 2020, 10, 6862-6869. (d) Li, Q.-Z.; Zeng, R.; Han, B.; Li, J.-L. Single-Electron Transfer Reactions Enabled by N-Heterocyclic Carbene Organocatalysis. Chem. - Eur. J. 2021, 27, 3238-3250. (e) Marzo, L. Recent Advances in Organic Synthesis Using Light-Mediated N-Heterocyclic Carbene Catalysis. Eur. J. Org. Chem. 2021, 2021, 4603. (8) (a) Thiophenes, Gronowitz, S.; Hörnfeldt, A.-B., Eds.; Academic Press: Oxford, 2004; (b) Modern Heterocyclic Chemistry, Alvarez-Builla, J.; Vaquero, J. J.; Barluenga, J., Eds.; Wiley-VCH: 2011; (c) Hunjan, M. K.; Panday, S.; Gupta, A.; Bhaumik, J.; Das, P.; Laha, J. K. Recent Advances in Functionalization of Pyrroles and their Translational Potential. Chem. Rec. 2021, 21, 715-780.
- (9) (a) Zhu, X.; Lin, Y.; Sun, Y.; Beard, M. C.; Yan, Y. Lead-Halide Perovskites for Photocatalytic α -Alkylation of Aldehydes. *J. Am. Chem. Soc.* **2019**, *141*, 733–738. (b) Dong, Y.; Li, R.; Zhou, J.; Sun, Z. Synthesis of Unsymmetrical 1,4-Dicarbonyl Compounds by Photo-

- catalytic Oxidative Radical Additions. *Org. Lett.* **2021**, 23, 6387–6390. (c) Goti, G.; Bieszczad, B.; Vega-Peñaloza, A.; Melchiorre, P. Stereocontrolled Synthesis of 1,4-Dicarbonyl Compounds by Photochemical Organocatalytic Acyl Radical Addition to Enals. *Angew. Chem., Int. Ed.* **2019**, 58, 1213–1217. (d) Sarkar, S.; Banerjee, A.; Yao, W.; Patterson, E. V.; Ngai, M.-Y. Photocatalytic Radical Aroylation of Unactivated Alkenes: Pathway to β-Functionalized 1,4-, 1,6-, and 1,7-Diketones. *ACS Catal.* **2019**, 9, 10358–10364.
- (10) Zhao, X.; Li, B.; Xia, W. Visible-Light-Promoted Photocatalyst-Free Hydroacylation and Diacylation of Alkenes Tuned by NiCl₂·DME. *Org. Lett.* **2020**, *22*, 1056–1061.
- (11) (a) Collett, C. J.; Massey, R. S.; Maguire, O. R.; Batsanov, A. S.; O'Donoghue, A. C.; Smith, A. D. Mechanistic Insights into the Triazolylidene-Catalysed Stetter and Benzoin Reactions: Role of the *N*-Aryl Substituent. *Chem. Sci.* **2013**, *4*, 1514–1522. (b) Barletta, G.; Huskey, W. P.; Jordan, F. Observation of a 2-α-enamine from a 2-(methoxyphenylmethyl)-3,4-dimethylthiazolium salt in water: implications for catalysis by thiamin diphosphate-dependent α-keto acid decarboxylases. *J. Am. Chem. Soc.* **1992**, *114*, 7607–7608.
- (12) (a) Regnier, V.; Romero, E. A.; Molton, F.; Jazzar, R.; Bertrand, G.; Martin, D. What Are the Radical Intermediates in Oxidative *N*-Heterocyclic Carbene Organocatalysis? *J. Am. Chem. Soc.* **2019**, *141*, 1109–1117. (b) Delfau, L.; Nichilo, S.; Molton, F.; Broggi, J.; Tomás-Mendivil, E.; Martin, D. Critical Assessment of the Reducing Ability of Breslow-type Derivatives and Implications for Carbene-Catalyzed Radical Reactions. *Angew. Chem., Int. Ed.* **2021**, *133*, 26783.
- (13) Contreras-García, J.; Johnson, E. R.; Keinan, S.; Chaudret, R.; Piquemal, J.-P.; Beratan, D. N.; Yang, W. NCIPLOT: A Program for Plotting Noncovalent Interaction Regions. *J. Chem. Theory Comput.* **2011**, *7*, 625–632.
- (14) (a) Horn, P. R.; Mao, Y.; Head-Gordon, M. Probing non-covalent interactions with a second-generation energy decomposition analysis using absolutely localized molecular orbitals. *Phys. Chem. Chem. Phys.* **2016**, *18*, 23067–23079. (b) Mao, Y.; Loipersberger, M.; Kron, K. J.; Derrick, J. S.; Chang, C. J.; Sharada, S. M.; Head-Gordon, M. Consistent inclusion of continuum solvation in energy decomposition analysis: theory and application to molecular CO₂ reduction catalysts. *Chem. Sci.* **2021**, *12*, 1398–1414.
- (15) Lu, T.; Chen, F. Multiwfn: A multifunctional wavefunction analyzer. *J. Comput. Chem.* **2012**, 33, 580–592.
- (16) Liu, Z.; Lu, T.; Chen, Q. An sp-hybridized all-carboatomic ring, cyclo[18]carbon: Electronic structure, electronic spectrum, and optical nonlinearity. *Carbon* **2020**, *165*, 461–467.
- (17) (a) Peach, M. J. G.; Sueur, C. R. L.; Ruud, K.; Guillaume, M.; Tozer, D. J. TDDFT diagnostic testing and functional assessment for triazene chromophores. *Phys. Chem. Chem. Phys.* **2009**, *11*, 4465–4470. (b) Muniz-Miranda, F.; Pedone, A.; Battistelli, G.; Montalti, M.; Bloino, J.; Barone, V. Benchmarking TD-DFT against Vibrationally Resolved Absorption Spectra at Room Temperature: 7-Aminocoumarins as Test Cases. *J. Chem. Theory Comput.* **2015**, *11*, 5371–5384. (c) Caricato, M.; Trucks, G. W.; Frisch, M. J.; Wiberg, K. B. Oscillator Strength: How Does TDDFT Compare to EOM-CCSD? *J. Chem. Theory Comput.* **2011**, *7*, 456–466.
- (18) Weinhold, F. Natural Bond Orbital Analysis: A Critical Overview of Relationships to Alternative Bonding Perspectives. *J. Comput. Chem.* **2012**, 33, 2363–2379.
- (19) Kaljurand, I.; Kütt, A.; Sooväli, L.; Rodima, T.; Mäemets, V.; Leito, I.; Koppel, I. A. Extension of the Self-Consistent Spectrophotometric Basicity Scale in Acetonitrile to a Full Span of 28 pK_a Units: Unification of Different Basicity Scales. *J. Org. Chem.* **2005**, *70*, 1019–1028.
- (20) In addition, the electron transfer may be mediated by an EDA complex between an electron acceptor substrate and hydrogen bond complex 20.